International Journal of Steel Structures 15(4): 809-826 (2015)
DOI 10.1007/s13296-015-1204-8
ISSN 1598-2351 (Print)
ISSN 2093-6311 (Online)

International Journal of
STEEL
STRUCTURES
www.springer.com/journal/13296

Influential Parameter Analysis on Vibration Responses of Rigid-frame Viaducts Induced by Running High-speed Trains

Liangming Sun[1,*], Toshiro Hayashikawa[2], Xingwen He[3], and Weiping Xie[4]

[1]*PhD, School of Civil Engineering and Architecture, Wuhan University of Technology, Wuhan, 430070, China*
[2]*Professor, Faculty of Engineering, Hokkaido University, Sapporo, 060-8628, Japan*
[3]*Assistant Professor, Faculty of Engineering, Hokkaido University, Sapporo, 060-8628, Japan*
[4]*Professor, School of Civil Engineering and Architecture, Wuhan University of Technology, Wuhan, 430070, China*

Abstract

This study is intended to clarify the parametric influence for the vibration responses of rigid-frame viaducts in both vertical and lateral directions caused by running high-speed trains. A developed 3D numerical analysis approach considering train-bridge interaction is applied to investigate the vibration characteristics of rigid-frame viaducts. The analytical model is composed of the high-speed train model with multi-DOFs vibration system for each car and the rigid-frame viaduct model with three bridge blocks. They are linked by an assumed wheel-rail relation through the rail model considering the simulated track irregularities. By using the analytical model, the parametric study is carried out. The impact factors including train speed, train type, track irregularity, rail type and damping are investigated and identified as significant variables. The analytical results are significant and give some instructive information regarding the impact factors of the train-bridge system which could be much helpful for the mitigation of vibration and the maintenance in the high-speed railway.

Keywords: Vibration response, rigid-frame viaduct, high-speed train, train-bridge interaction, impact factor

1. Introduction

With the rapid economic and urban development, the high-speed railway connecting major cities serves as a vital role in the national transportation network. It becomes a new trend of railway development in the world due to its high speed, comfort, punctuality, safety, less land use and so on. Among the high-speed railways, the bridges take a great percentage. We are deriving the benefits of high-speed railways in developed regions in the world. However, the problems of bridge vibration induced by running high-speed trains (HSTs) have become more prominent in recent years (Matsuura, 1976; Frýba, 1996; Yang *et al*., 2004). Through the continuous increase of train speeds, the extensive application of high performance materials, the ever-increasing span length of bridges, and the improvement of vibration environment along the high-speed railway, all attribute to the related problems caused by bridge vibration. The bridge vibration may increase the internal force of structures, produce vibration deformation, cause local fatigue damage of structural members and even completely destroy the bridges (Uno *et al*., 2007; Miyashita *et al*., 2007; Xia *et al*., 2012; Zhou *et al*., 2013; Liu *et al*., 2013). They can propagate to the ambient ground via the footing and pile structures, thereby generating long-term ground vibration, bringing annoyances to the residents alongside and malfunctioning to the vibration-sensitive equipment when the HSTs pass through developed areas or high-tech industrial areas (Yokoshima and Tamura, 1999; Ju *et al*., 2007; Xia *et al*., 2009). Therefore, the HST-induced vibration has become a more serious concern to people along with the further development of the high-speed railway.

Regarding HST-induced bridge vibration, the dynamic behavior of railway bridges has been a key research subject of bridge design and maintenance since Tokaido Shinkansen was the first high-speed railway to begin operation from 1964 in the world. Basic theories for the dynamics of railway bridges caused by running HSTs were widely investigated by a number of researchers (Matsuura, 1976; Frýba, 1996; Yang *et al*., 2004; Garinei and Risitano, 2008; Xia *et al*., 2012; Olmos and Astiz, 2013). Analytical models of the coupled TBI system together with experimental validations and engineering applications in the high-speed railways have been studied

Received December 13, 2014; accepted May 28, 2015;
published online December 31, 2015

*Corresponding author
Tel: +86-13545909941, Fax: +86-27-87664561
E-mail: sunliangming@gmail.com

by Tanabe *et al.* (2003), Yang and Lin (2005), Uno *et al.* (2007), Dinh *et al.* (2009), Martínez-Rodrigo (2010), Guo *et al.* (2012), Xie and Xu (2012), Rezvani *et al.* (2013) among others. Based on these studies, the vertical and lateral dynamic responses of railway bridges, and the safety and stability of HSTs during transit, have been studied and many useful results were obtained and reported. However, most of these studies were focused on solving the TBI problem of simple-supported girder bridges, few studies have been done for that of rigid-frame viaducts (RFVs) but also investigated the vibration influence of various impact factors in the world.

In Japan, the RFV as one of bridge structure types is widely applied among the high-speed railways. Some studies were carried out by means of field measurements and numerical simulations. For instance, Wakui *et al.* (1995), Kawatani *et al.* (2006) and Su *et al.* (2010) mainly focused on a three-dimensional analytical approach to study the TBI problem of the RFVs at a certain speed. Wakui *et al.* (1995) analyzed only vertical deflection at the second mid-span; Kawatani *et al.* (2006) clarified only vertical vibration accelerations of three points at the hanging part, the top of first pier and third pier; Su *et al.* (2010) investigated only vibration accelerations of three directions at the top of one pier. But they did not further discuss the vibration influence of various parameters for the RFVs. Takemiya and Bian (2007) mainly focused on studying the ground vibration around Shinkansen viaducts under moving axle loads although they presented the time histories of viaduct displacements. From the above studies, it is clear that HST-induced vibration properties of RFVs haven't been fully explored, especially the vibration influence of various parameters. They are different from those of simple-supported girder bridges because of different structure types. Therefore, it is necessary to study the TBI problem in detail in order to offer convenient predictions and diagnoses to the HST-induced vibrations of either existing bridges or those in the planning stage and get some instructive information regarding the various parameters of TBI system.

In this study, focusing on a standard type of high-speed railway viaduct in Tokaido Shinkansen, the vibration characteristics and the parametric influences for the RFVs are investigated by applying developed 3D numerical analysis approach considering train-bridge interaction. The analytical model is composed of the HST model with multi-DOFs vibration system for each car and the RFV model with three bridge blocks. They are linked by an assumed wheel-rail relation through the rail model considering the simulated track irregularities. By using the analytical model, the parametric study is carried out to clarify the effects of various impact factors including train speed, train type, track irregularity, rail type and damping. Simultaneously, the vibration responses of RFVs are evaluated by the maximum acceleration and the VAL. Because the RFVs are often so adjacent to residences or important facilities in major urban areas, the vibration problems induced by running HSTs have been given more attention along with the further development of high-speed railway. It is inevitable to take into account various impact factors to investigate the vibration characteristics to guide how to mitigate the HST-induced vibration.

2. Analytical Model of the TBI System

The analytical model of the TBI system is composed of three subsystems which are a high-speed train model, a rail model and a rigid-frame viaduct model. The HST model consists of several passenger carriages, and the RFV model consists of the viaducts of reinforced concrete in the form of a portal rigid frame. They are linked by an assumed wheel-rail relation through the rail model. The simulated track irregularities are also considered as the internal self-excitation of this TBI system. In the coordinate system of TBI system, the longitudinal, lateral and vertical directions are denoted as the x, y and z axes, respectively.

2.1. High-speed train model

For Tokaido Shinkansen, many more HSTs have been put into service and the current number of HSTs is five times greater than that of the initial stage. The operational speed has been increased from 210 km/h at the beginning to 270 km/h at present. In this analysis, the HST model selects 300 Series composed of sixteen cars as the analytical object based on actual operational conditions. Each car is treated as a car body, two bogies and four wheelsets connected by spring-dashpot suspension devices, and modeled as a complicated multi-DOFs vibration system without the coupling device as shown in Fig. 1. The vibration properties of HSTs are shown in Table 1. To simplify the analysis but retain its accuracy, the assumption is considered as follows: the HST is running on a straight line at a constant speed, neither accelerating nor decelerating; the wheelsets remain in full contact with the rail at all times (i.e., no jumps occur) and move with the two rails in both vertical and lateral directions; the uniform HST model is used to describe all of train carriages without taking into account the differences between locomotive carriages and normal passenger carriages; the car body, bogies and wheelsets in each car are regarded as rigid components, neglecting their elastic deformation during vibration; the connections between the car body, bogies and wheelsets are represented three-dimensionally by two groups of spring-dashpot suspension devices that are linear springs and viscous dashpots. Therefore, this HST model can appropriately express the vibration responses of TBI system in both vertical and lateral directions. Its vibration differential equations are shown as follows:

(1) Vibration differential equations of the car body
Lateral translation of the car body:

$$m_1\ddot{y}_{j1}-\sum_{l=1}^{2}\sum_{m=1}^{2}(-1)^m\{k_2[-(-1)^m y_{j1}-(-1)^m\lambda_{z1}\theta_{jx1}+(-1)^{l+m}\lambda_{x1}\theta_{jz1}+(-1)^m y_{j2l}-(-1)^m\lambda_{z2}\theta_{jx2l}]$$
$$+c_2[-(-1)^m\dot{y}_{j1}-(-1)^m\lambda_{z1}\dot{\theta}_{jx1}+(-1)^{l+m}\lambda_{x1}\dot{\theta}_{jz1}+(-1)^m\dot{y}_{j2l}-(-1)^m\lambda_{z2}\dot{\theta}_{jx2l}]\}=0 \quad (1)$$

Bouncing of the car body:

$$m_1\ddot{z}_{j1}+\sum_{l=1}^{2}\sum_{m=1}^{2}\{k_3[z_{j1}+(-1)^l\lambda_{x1}\theta_{jy1}-(-1)^m\lambda_{y3}\theta_{jx1}-z_{j2l}+(-1)^m y_{y3}\theta_{jx2l}]$$
$$+c_3[\dot{z}_{j1}+(-1)^l\lambda_{x1}\dot{\theta}_{jy1}-(-1)^m\lambda_{y3}\dot{\theta}_{jx1}-\dot{z}_{j2l}+(-1)^m\lambda_{z3}\dot{\theta}_{jx2l}]\}=0 \quad (2)$$

Rolling of the car body:

$$I_{x1}\ddot{\theta}_{jx1}-\sum_{l=1}^{2}\sum_{m=1}^{2}(-1)^m\lambda_{y3}\{k_3[z_{j1}+(-1)^l\lambda_{x1}\theta_{jy1}-(-1)^m\lambda_{y3}\theta_{jx1}-z_{j2l}+(-1)^m y_{y3}\theta_{jx2l}]$$
$$+c_3[\dot{z}_{j1}+(-1)^l\lambda_{x1}\dot{\theta}_{jy1}-(-1)^m\lambda_{y3}\dot{\theta}_{jx1}-\dot{z}_{j2l}+(-1)^m\lambda_{z3}\dot{\theta}_{jx2l}]\}$$
$$-\sum_{l=1}^{2}\sum_{m=1}^{2}(-1)^m\lambda_{z1}\{k_2[-(-1)^m\lambda_{j1}-(-1)^m\lambda_{z1}\theta_{jx1}+(-1)^{l+m}\lambda_{x1}\theta_{jz1}+(-1)^m y_{j2l}-(-1)^m\lambda_{z2}\theta_{jx2l}]$$
$$+c_2[-(-1)^m\dot{y}_{j1}-(-1)^m\lambda_{z1}\dot{\theta}_{jx1}+(-1)^{l+m}\lambda_{x1}\dot{\theta}_{jz1}+(-1)^m\dot{y}_{j2l}-(-1)^m\lambda_{z2}\dot{\theta}_{jx2l}]\}=0 \quad (3)$$

Pitching of the car body:

$$I_{y1}\ddot{\theta}_{jy1}+\sum_{l=1}^{2}\sum_{m=1}^{2}(-1)^l\lambda_{x1}\{k_3[z_{j1}+(-1)^l\lambda_{x1}\theta_{jy1}-(-1)^m\lambda_{y3}\theta_{jx1}-z_{j2l}+(-1)^m y_{y3}\theta_{jx2l}]$$
$$+c_3[\dot{z}_{j1}+(-1)^l\lambda_{x1}\dot{\theta}_{jy1}-(-1)^m\lambda_{y3}\dot{\theta}_{jx1}-\dot{z}_{j2l}+(-1)^m\lambda_{y3}\dot{\theta}_{jx2l}]\}=0 \quad (4)$$

Yawing of the car body:

$$I_{z1}\ddot{\theta}_{jz1}+\sum_{l=1}^{2}\sum_{m=1}^{2}(-1)^{l+m}\lambda_{x1}\{k_2[-(-1)^m y_{j1}-(-1)^m\lambda_{z1}\theta_{jx1}+(-1)^{l+m}\lambda_{x1}\theta_{jz1}+(-1)^m y_{j2l}-(-1)^m\lambda_{z2}\theta_{jx2l}]$$
$$+c_2[-(-1)^m\dot{y}_{j1}-(-1)^m\lambda_{z1}\dot{\theta}_{jx1}+(-1)^{l+m}\lambda_{x1}\dot{\theta}_{jz1}+(-1)^m\dot{y}_{j2l}-(-1)^m\lambda_{z2}\dot{\theta}_{jx2l}]\}$$
$$+\sum_{l=1}^{2}\sum_{m=1}^{2}(-1)^m\lambda_{y4}k_1[(-1)^m\lambda_{y4}(\theta_{jz1}-\theta_{jz2l})]=0 \quad (5)$$

(2) Vibration differential equations of train bogies
Sway of the front or rear bogie:

$$m_2\ddot{y}_{j2l}+\sum_{m=1}^{2}(-1)^m\{k_2[-(-1)^m y_{j1}-(-1)^m\lambda_{z1}\theta_{jx1}+(-1)^{l+m}\lambda_{x1}\theta_{jz1}+(-1)^m y_{j2l}-(-1)^m\lambda_{z2}\theta_{jx2l}]$$
$$+c_2[-(-1)^m\dot{y}_{j1}-(-1)^m\lambda_{z1}\dot{\theta}_{jx1}+(-1)^{l+m}\lambda_{x1}\dot{\theta}_{jz1}+(-1)^m\dot{y}_{j2l}-(-1)^m\lambda_{z2}\dot{\theta}_{jx2l}]\}$$
$$-\sum_{k=1}^{2}\sum_{m=1}^{2}(-1)^m k_{22}[-(-1)^m y_{j2l}-(-1)^m\lambda_{z3}\theta_{jx2l}+(-1)^{k+m}\lambda_{x2}\theta_{jz2l}+(-1)^m y_{j3lk}]=0 \quad (6)$$

Parallel hop of the front or rear bogie:

$$m_2\ddot{z}_{j2l}-\sum_{m=1}^{2}\{k_3[z_{j1}+(-1)^l\lambda_{x1}\theta_{jy1}-(-1)^m\lambda_{y3}\theta_{jx1}-z_{j2l}+(-1)^m\lambda_{y3}\theta_{jx2l}]$$
$$+c_3[\dot{z}_{j1}+(-1)^l\lambda_{x1}\dot{\theta}_{jy1}-(-1)^m\lambda_{y3}\dot{\theta}_{jx1}-\dot{z}_{j2l}+(-1)^m\lambda_{y3}\dot{\theta}_{jx2l}]\}$$
$$+\sum_{k=1}^{2}\sum_{m=1}^{2}\{k_{23}[z_{j2l}-(-1)^m\lambda_{y2}\theta_{jx2l}+(-1)^k\lambda_{x2}\theta_{jy2l}-z_{j3lk}+(-1)^m\lambda_{y2}\theta_{jx3lk}]$$
$$+c_{23}[\dot{z}_{j2l}-(-1)^m\lambda_{y2}\dot{\theta}_{jx2l}+(-1)^k\lambda_{x2}\dot{\theta}_{jy2l}-\dot{z}_{j3lk}+(-1)^m\lambda_{y2}\dot{\theta}_{jx3lk}]\}=0 \quad (7)$$

Axle tramp of the front or rear bogie:

$$I_{x2}\ddot{\theta}_{jx2l}-\sum_{m=1}^{2}(-1)^m\lambda_{z2}\{k_2[-(-1)^m y_{j1}-(-1)^m\lambda_{z1}\theta_{jx1}+(-1)^{l+m}\lambda_{x1}\theta_{jz1}+(-1)^m y_{j2l}-(-1)^m\lambda_{z2}\theta_{jx2l}]$$
$$+c_2[-(-1)^m\dot{y}_{j1}-(-1)^m\lambda_{z1}\dot{\theta}_{jx1}+(-1)^{l+m}\lambda_{x1}\dot{\theta}_{jz1}+(-1)^m\dot{y}_{j2l}-(-1)^m\lambda_{z2}\dot{\theta}_{jx2l}]\}$$
$$+\sum_{m=1}^{2}(-1)^m\lambda_{y3}\{k_3[z_{j1}+(-1)^l\lambda_{x1}\theta_{jy1}-(-1)^m\lambda_{y3}\theta_{jx1}-z_{j2l}+(-1)^m\lambda_{y3}\theta_{jx2l}]$$
$$+c_3[\dot{z}_{j1}+(-1)^l\lambda_{x1}\dot{\theta}_{jy1}-(-1)^m\lambda_{y3}\dot{\theta}_{jx1}-\dot{z}_{j2l}+(-1)^m\lambda_{y3}\dot{\theta}_{jx2l}]\}$$
$$-\sum_{k=1}^{2}\sum_{m=1}^{2}(-1)^m\lambda_{z3}k_{22}[-(-1)^m y_{j2l}-(-1)^m\lambda_{z3}\theta_{jx2l}+(-1)^{k+m}\lambda_{x2}\theta_{jz2l}+(-1)^m y_{j3lk}]$$
$$-\sum_{k=1}^{2}\sum_{m=1}^{2}(-1)^m\lambda_{y2}\{k_{23}[z_{j2l}-(-1)^m\lambda_{y2}\theta_{jx2l}+(-1)^k\lambda_{x2}\theta_{jy2l}-z_{j3lk}+(-1)^m\lambda_{y2}\theta_{jx3lk}]$$
$$+c_{23}[\dot{z}_{j2l}-(-1)^m\lambda_{y2}\dot{\theta}_{jx2l}+(-1)^k\lambda_{x2}\dot{\theta}_{jy2l}-\dot{z}_{j3lk}+(-1)^m\lambda_{y2}\dot{\theta}_{jx3lk}]\}=0 \quad (8)$$

Windup motion of the front or rear bogie:

$$I_{y2}\ddot{\theta}_{jy2l}-\sum_{k=1}^{2}\sum_{m=1}^{2}(-1)^k\lambda_{z3}k_{21}(-1)^{k+m}\lambda_{y2}\theta_{jz2l}$$
$$+\sum_{k=1}^{2}\sum_{m=1}^{2}(-1)^k\lambda_{x2}\{k_{23}[z_{j2l}-(-1)^m\lambda_{y2}\theta_{jx2l}+(-1)^k\lambda_{x2}\theta_{jy2l}-z_{j3lk}+(-1)^m\lambda_{y2}\theta_{jx3lk}]$$
$$+c_{23}[\dot{z}_{j2l}-(-1)^m\lambda_{y2}\dot{\theta}_{jx2l}+(-1)^k\lambda_{x2}\dot{\theta}_{jy2l}-\dot{z}_{j3lk}+(-1)^m\lambda_{y2}\dot{\theta}_{jx3lk}]\}=0 \quad (9)$$

Yawing of the front or rear bogie:

$$I_{z2}\ddot{\theta}_{jz2l}-\sum_{m=1}^{2}(-1)^m\lambda_{y4}k_1[(-1)^m\lambda_{y4}(\theta_{jz1}-\theta_{jz2l})]+\sum_{k=1}^{2}\sum_{m=1}^{2}(-1)^{k+m}\lambda_{y2}k_{21}(-1)^{k+m}\lambda_{y2}\theta_{jz2l}$$
$$+\sum_{k=1}^{2}\sum_{m=1}^{2}(-1)^{k+m}\lambda_{x2}k_{22}[-(-1)^m y_{j2l}-(-1)^m\lambda_{z3}\theta_{jx2l}+(-1)^{k+m}\lambda_{x2}\theta_{jz2l}+(-1)^m y_{j3lk}]=0 \quad (10)$$

(3) Vibration differential equations of train wheel-sets
Lateral displacement of the wheel-sets:

$$m_3\ddot{y}_{j3lk}+\sum_{m=1}^{2}(-1)^m k_{22}[-(-1)^m y_{j2l}-(-1)^m\lambda_{z3}\theta_{jx2l}+(-1)^{k+m}\lambda_{x2}\theta_{jz2l}+(-1)^m y_{j3lk}]=-\sum_{m=1}^{2}P_{jylkm}(t) \quad (11)$$

Vertical displacement of the wheel-sets:

$$m_3\ddot{z}_{j3lk}-\sum_{m=1}^{2}\{k_{23}[z_{j2l}-(-1)^m\lambda_{y2}\theta_{jx2l}+(-1)^k\lambda_{x2}\theta_{jy2l}-z_{j3lk}+(-1)^m y_{y2}\theta_{jx3lk}]$$

$$+c_{23}[\dot{z}_{j2l}-(-1)^m\lambda_{y2}\dot{\theta}_{jx2l}+(-1)^k\lambda_{x2}\dot{\theta}_{jy2l}-\dot{z}_{j3lk}+(-1)^m\lambda_{y2}\dot{\theta}_{jx3lk}]\}=-\sum_{m=1}^{2}P_{jzlkm}(t) \tag{12}$$

Rolling of the wheel-sets:

$$I_{x3}\ddot{\theta}_{jx3lk}+\sum_{m=1}^{2}(-1)^m\lambda_{y2}\{k_{23}[z_{j2l}-(-1)^m\lambda_{y2}\theta_{jx2l}+(-1)^k\lambda_{x2}\theta_{jy2l}-z_{j3lk}+(-1)^m\lambda_{y2}\theta_{jx3lk}]$$

$$+c_{23}[\dot{z}_{j2l}-(-1)^m\lambda_{y2}\dot{\theta}_{jx2l}+(-1)^k\lambda_{x2}\dot{\theta}_{jy2l}-\dot{z}_{j3lk}+(-1)^m\lambda_{y2}\dot{\theta}_{jx3lk}]\}=-r\sum_{m=1}^{2}P_{jylkm}(t)+(-1)^m\lambda_{y1}\sum_{m=1}^{2}P_{jzlkm}(t) \tag{13}$$

Herein, the subscript j indicates the sequence number of the car. The subscripts relative to the motion of the train are described as: l=1, 2 indicate the front and rear bogies; m=1, 2 indicate the left and right sides of the train, k=1, 2 indicate the front and rear axles of the bogie, respectively. $P_{jylkm}(t)$ and $P_{jzlkm}(t)$ respectively represent the dynamic wheel loads acting on the structure in the lateral direction and vertical direction, which are represented as follows:

$$P_{jylkm}(t)=-m_3\ddot{w}_{jylkm}/2-(-1)^m k_{22}[-(-1)^m y_{j2l}-(-1)^m\lambda_{z3}\theta_{jx2l}+(-1)^{k+m}\lambda_{x2}\theta_{jz2l}+(-1)^m y_{j3lk}] \tag{14}$$

$$P_{jzlkm}(t)=-(m_1g/8+m_2g/4+m_3g/2)-m_3\ddot{w}_{jzlkm}/2+\{k_{23}[z_{j2l}-(-1)^m\lambda_{y2}\theta_{jx2l}+(-1)^k\lambda_{x2}\theta_{jy2l}-z_{j3lk}+(-1)^m\lambda_{y2}\theta_{jx3lk}]$$
$$+c_{23}[\dot{z}_{j2l}-(-1)^m\lambda_{y2}\dot{\theta}_{jx2l}+(-1)^k\lambda_{x2}\dot{\theta}_{jy2l}-\dot{z}_{j3lk}+(-1)^m\lambda_{y2}\dot{\theta}_{jx3lk}]\} \tag{15}$$

where the variables w_{jylkm} and w_{jzlkm} denote the sum of the displacements and track irregularities of the rail in the lateral and vertical directions, respectively; g is the acceleration of gravity.

Expanding the equations described above, the differential equations of the HST model can be expressed in matrix form as follows.

$$\mathbf{M}_t\ddot{\mathbf{w}}_t+\mathbf{C}_t\dot{\mathbf{w}}_t+\mathbf{K}_t\mathbf{w}_t=\mathbf{f}_t \tag{16}$$

Herein, $\mathbf{M}_t$, $\mathbf{C}_t$, $\mathbf{K}_t$ and $\mathbf{f}_t$, respectively, denote the mass,

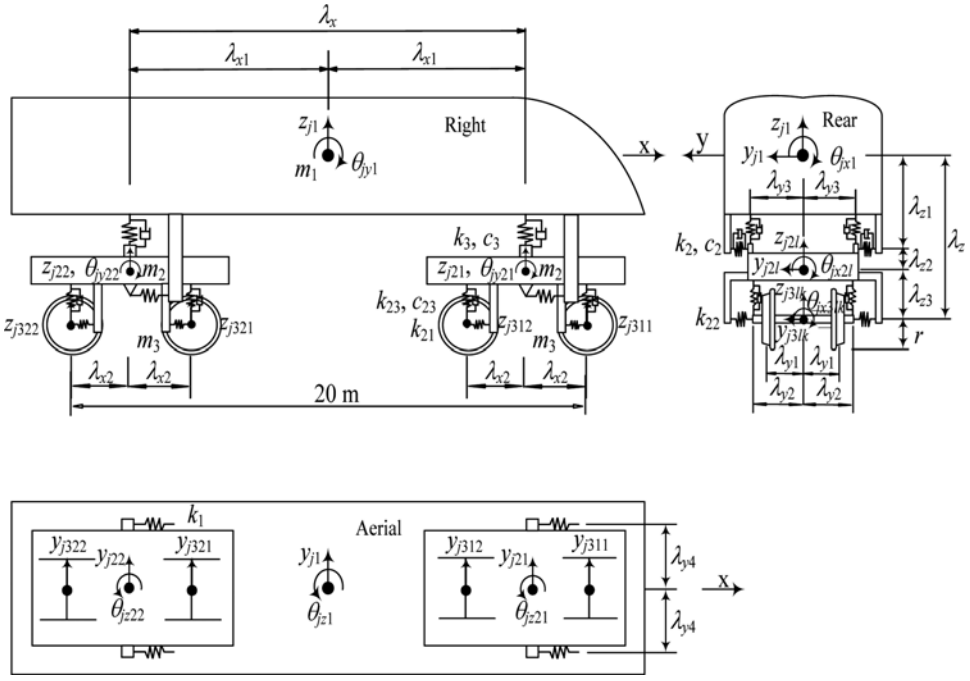

Figure 1. High-speed train model for vibration analysis.

Table 1. Vibration properties of high-speed trains

Definition		Notation	Type	
			300 Series	0 Series
Mass (t)	car body	m_1	32.818	36.68
	bogie	m_2	2.639	5.98
	wheel	m_3	0.9025	1.465
Mass moment of inertia (kN·s^2·m)	car body	I_{x1}	49.248	477.358
		I_{y1}	2512.628	8381.94
		I_{z1}	2512.628	8381.94
	bogie	I_{x2}	2.909	42.238
		I_{y2}	4.123	84.378
		I_{z2}	4.123	84.378
	wheelset	I_{x3}	0.885	16.17
Spring constant (kN/m)	upper	k_1	5000.0	17640.0
		k_2	176.4	323.4
		k_3	443.0	426.3
	lower	k_{21}	17500.0	15000.0
		k_{22}	4704.0	17150.0
		k_{23}	1209.81	1113.0
Damping coefficient (kN·s/m)	upper	c_2	39.2	29.4
		c_3	21.6	19.6
	lower	c_{23}	19.6	14.7

damping, stiffness matrices and the external force vector of the HST system, which can be derived by expanding those formulae of the HST described above.

2.2. Rigid-frame viaduct model

A Japanese high-speed railway viaduct is employed as shown in Fig. 2, which is a typical reinforced concrete viaduct in the form of a rigid portal frame. This RFV as one of bridge structure types is widely applied in the high-speed railways in Japan. When the HST is running over the RFV, the forces from the wheels are transmitted to the bridge slab through the rail. In this study, it assumed that there is no relative displacement between the rail and bridge slab, furthermore, the rails are always continuously set upon the slab. The RFVs are built with 24 m length bridge blocks which are separated from adjacent ones and connected with each other only by rail structure and ballast at adjacent ends. Each block consists of three 6 m length center spans and two 3 m length cantilever girders, so called hanging parts, at each end. In consideration of the connecting effect of rail structure and the influence of train's entering and leaving, three blocks of RFVs are adopted for the analysis and modeled as 3D beam elements with six DOFs at each node as shown in Fig. 3. Only the vibration response of the middle block will be examined. The primary frequency of vertical and lateral mode for the middle block of the viaducts is respectively 11.9 and 2.2 Hz. The lumped mass system which incorporates the mass of the ballast is adopted for the beam elements. Since the HST runs between the piers of RFVs, the vibration of cantilever slabs in the transverse direction is not important. Therefore, they are not modeled with finite elements to reduce the number of nodes and

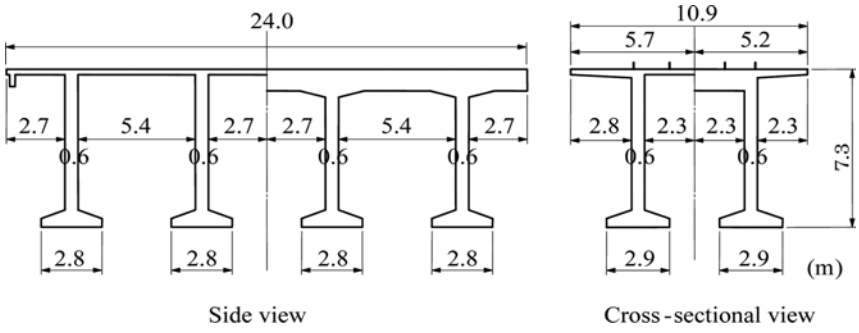

Figure 2. Dimensions of rigid-frame viaducts.

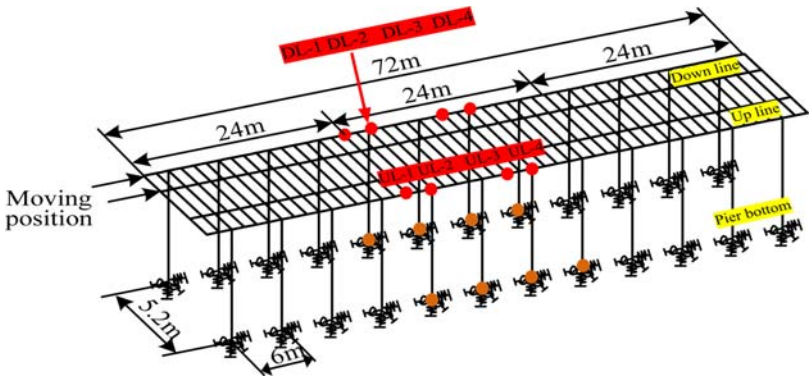

Figure 3. The rigid-frame viaduct model for vibration analysis.

Table 2. The constants of ground springs

Sort of spring	Longitudinal	Transverse
Vertical spring of pile top (kN/m)	3.86×10^6	
Rotating spring of pile top (kN·m/rad)	3.64×10^6	2.42×10^6
Horizontal spring of footing (kN/m)	4.84×10^3	4.72×10^3
Horizontal spring of pile top (kN/m)	8.22×10^4	8.08×10^4

their masses are added to the outside nodes of the slabs. On the other hand, the cantilever slabs in the longitudinal direction play an important role in bridge vibration and are modeled as 3D beam elements with the same length as sleeper intervals, which can express the vibration caused by the rail fastening distance. Double nodes defined as two independent nodes sharing the same coordinate are adopted at the pier bottoms to simulate the effect of ground springs. Ground springs are calculated according to the design codes including the elastic effects of the footing and pile structures as well as the surrounding soil. Their constants are shown in Table 2 (Kawatani *et al.*, 2006). Rayleigh damping is adopted for the structural model and damping constant 3% is assumed for the first and second modes of the structure according to the past field test results (Nishimura, 1990).

2.3. Rail model and track irregularity

The rail structure is modeled as 3D beam elements with six DOFs at each node. Double nodes are defined here to simulate the elastic effect of the sleepers and ballast at the positions of the sleepers. Structural properties of the rails are shown in Table 3. The vertical spring constant of the track is derived from the ratio of the wheel load to the

Table 3. Structural properties of the rails

Definition	Type	
	60 kg	70 kg
Mass (kg/m)	60.80	69.50
Cross-sectional area (cm^2)	77.50	88.16
Moment of inertia (cm^4)	3090	4311
Torsional constant (cm^4)	400	560

rail's displacement in the vertical direction. The horizontal spring constant is assumed to be 1/3 of the value in the vertical direction (Nishimura, 1990). Track irregularities in both vertical and lateral directions are also taken into account in this analysis. Because track irregularities and running HSTs are considered to be the most important source of excitation for the vibration analysis of TBI system. In general, the actual measured track irregularity record is necessary for the specific engineering if a simulation is expected to give a real response result and capture the influence of track irregularities. But it is not always available for the viaducts considered in a simulation. Another solution is to use a power spectral density (PSD) function for the track geometry in the frequency domain to represent the track irregularity. In this study, the PSD functions used for the vertical irregularity and lateral irregularity are given in Eqs. (17) and (18), respectively (Matsuura, 1998). The stochastic process samples of track irregularities are simulated by the frequency domain method (Chen and Zhai, 1999). Track irregularity spectra and simulated profile samples are shown in Fig. 4.

$$S_v(f)=2\times10^{-9}/f^3 \quad \text{m}^2/(1/\text{m}) \tag{17}$$

$$S_a(f)=10^{-9}/f^3 \quad \text{m}^2/(1/\text{m}) \tag{18}$$

In which, f (1/m) indicates the spatial frequency of the track irregularity.

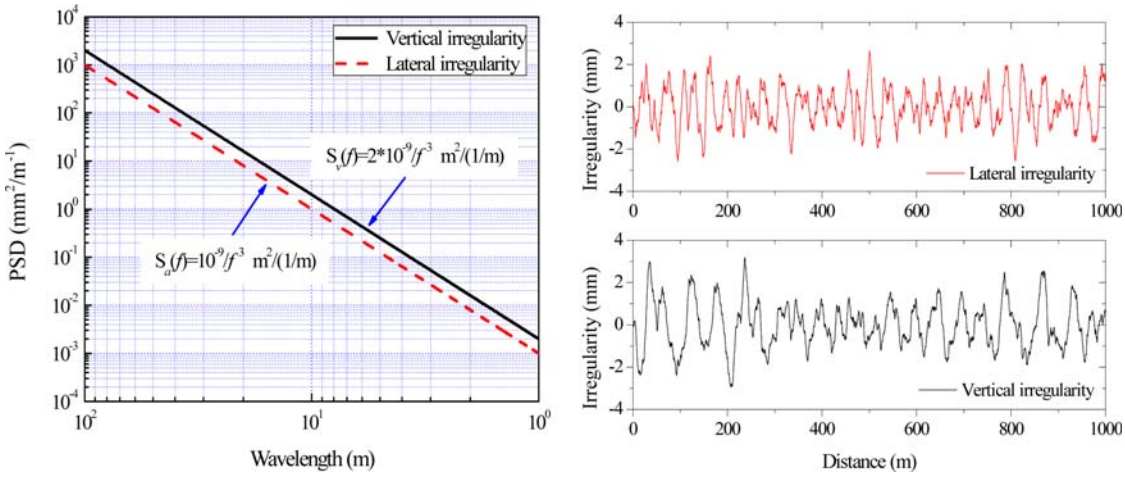

Figure 4. Track irregularity spectra and simulated profile samples.

3. Analytical Method for the TBI System

The coupled vibration responses of TBI system are analyzed considering train-bridge interaction based on the computer program. The vibration behavior of TBI system is a complex coupled time-varying vibration problem. Such this problem is generally solved by a numerical simulation based on a vibration interaction model for the whole TBI system. The vibration responses of RFVs induced by running HSTs result from several main factors, such as train speed, train type, track irregularity, rail type, damping, etc. Theoretically, the analytical model for the TBI system is mainly composed of the HST and the RFV, each of them characterized by some vibration differential equations. Newmark's β numerical integration method is applied to solve the coupled vibration differential equations of TBI system which is described in Eq. (19). Adopting 1/4 as the value of β, the vibration responses can be obtained accurately, with less than 1/1000 error for acceleration at each time step. The validity of the models and procedure is demonstrated through comparing analytical results with experimental ones (Sun, 2014). Considering the extremely high speed of the HST, the integral time step interval is set to 0.0005s.

$$\begin{bmatrix} \boldsymbol{M}_b & \boldsymbol{M}_{bt} \\ \text{Sym.} & \boldsymbol{M}_t \end{bmatrix} \begin{Bmatrix} \ddot{w}_b \\ \ddot{w}_t \end{Bmatrix} + \begin{bmatrix} \boldsymbol{C}_b & \boldsymbol{C}_{bt} \\ \text{Sym.} & \boldsymbol{C}_t \end{bmatrix} \begin{Bmatrix} \dot{w}_b \\ \dot{w}_t \end{Bmatrix} + \begin{bmatrix} \boldsymbol{K}_b & \boldsymbol{K}_{bt} \\ \text{Sym.} & \boldsymbol{K}_t \end{bmatrix} \begin{Bmatrix} w_b \\ w_t \end{Bmatrix} = \begin{Bmatrix} \boldsymbol{F}_b \\ \boldsymbol{F}_t \end{Bmatrix} \tag{19}$$

where $\boldsymbol{M}_b$, $\boldsymbol{C}_b$, and $\boldsymbol{K}_b$, respectively, denote the mass, damping and stiffness matrices of the RFV system, while $\boldsymbol{M}_{bt}$, $\boldsymbol{C}_{bt}$, $\boldsymbol{K}_{bt}$ and the symmetrical parts indicate the coupled components of TBI system. $\boldsymbol{w}_b$ and $\boldsymbol{w}_t$, compose the generalized displacement vector, while $\boldsymbol{F}_b$ and $\boldsymbol{F}_t$ compose the external force vector of TBI system. They can be derived by expanding the formulae of TBI system and the detailed formulation process can be found in the reference (Sun, 2014).

4. Vibration Response Analysis of the RFVs

In this study, taking advantage of the developed analytical procedure, the vibration behavior of RFVs caused by running HSTs at the operational speed of 270 km/h is discussed. In general, the vibration characteristics should be considered about some vibration parameters including vibration duration, direction, intensity and frequency. The observation points are shown in Fig. 4 such as DL-1, DL-2, DL-3 and DL-4, which, respectively, are the hanging part, the top of first pier, the central point and the top of third pier of the middle block of RFVs in the down line, with respect to the direction that the HSTs run towards. Their frequency characteristics are clarified by means of Fourier spectral analysis and 1/3 octave band spectral analysis.

4.1. Time histories and Fourier spectra

Time histories and Fourier spectra of acceleration responses of RFVs in both vertical and lateral directions are shown in Figs. 5 and 6, respectively. Their Max and RMS values are also indicated in these figures. About vibration duration, it is mainly determined by the speed of the HST and

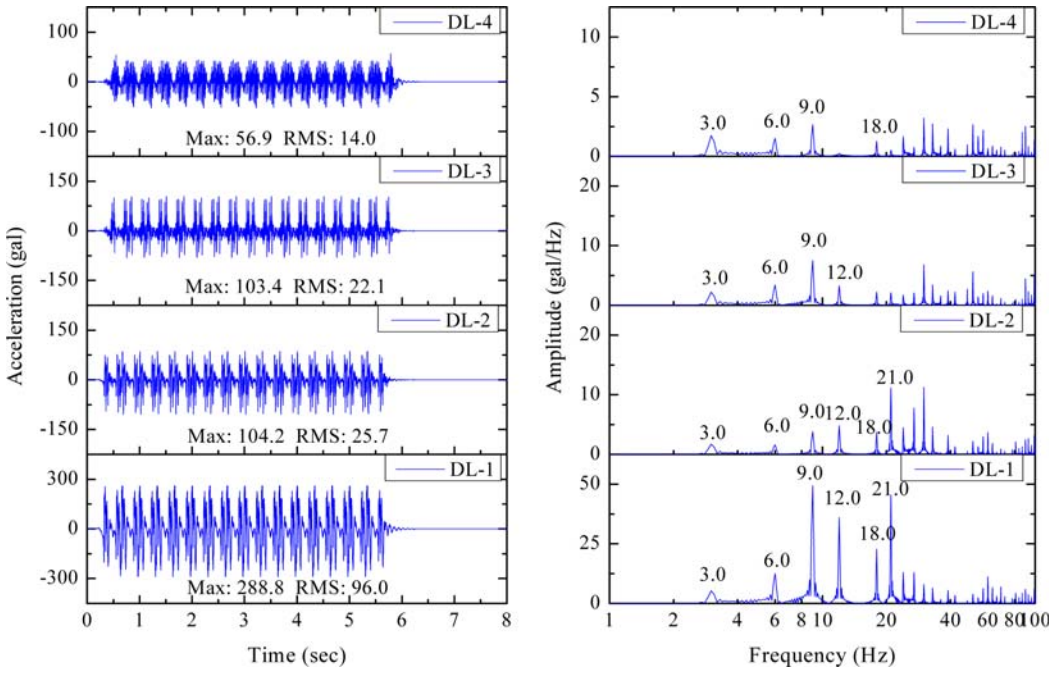

Figure 5. Time histories and Fourier spectra of acceleration responses of RFVs (Vertical).

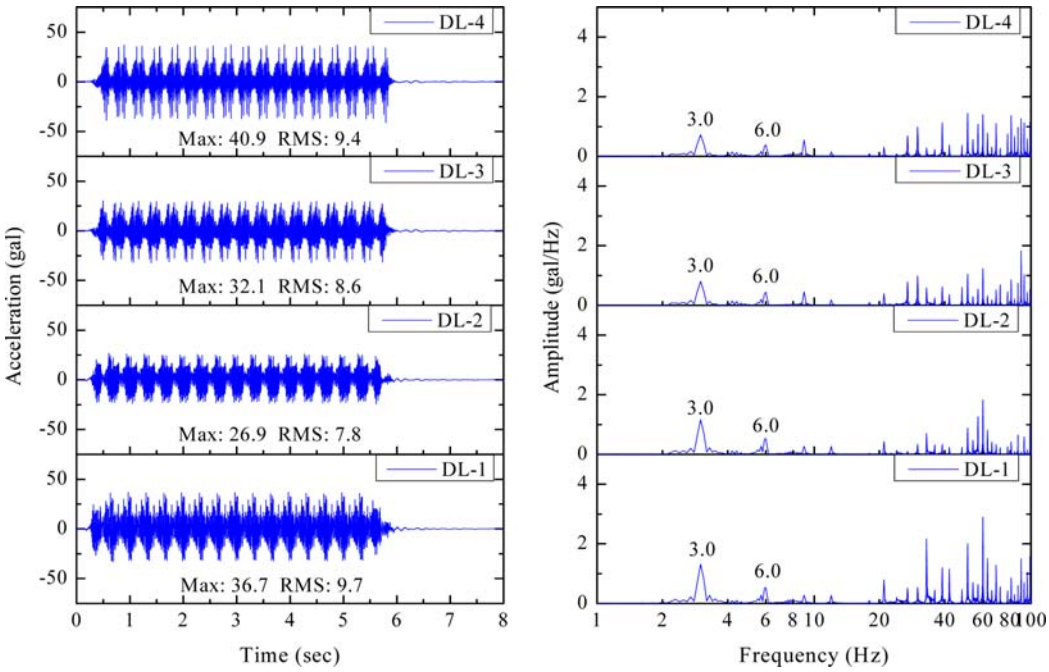

Figure 6. Time histories and Fourier spectra of acceleration responses of RFVs (Lateral).

departure frequency. Each time history consists of seventeen blocks of vibration among these results as well as the first and last blocks of vibration is the half of middle blocks of vibration. That is because the HST has sixteen cars altogether and the span of the RFVs is 6 m. When the HST is passing the RFVs, the adjacent two bogies for the adjacent two cars will induce coupled vibration response but the front and rear bogies for a car will induce isolated vibration response. About vibration direction, the vertical vibration responses are obviously larger than the lateral ones by comparing Max and RMS values but the frequency components are similar in both vertical and lateral directions. That is because the vertical excitations include the running HST and the vertical irregularity but the lateral excitation mainly includes the lateral irregularity. The gravity loads of HST mainly produce the vertical vibration responses. Therefore, many researchers only discuss the vertical vibration responses by using the gravity loads of HST, in most cases, without considering track irregularities. It is demonstrated that the vibration influence in the vertical direction is much bigger than that in the lateral direction for the RFVs.

About vibration intensity, the Max value of DL-1 is much larger than that of other parts especially at the central point DL-3 in the vertical direction. The predominant vibration response occurs at the hanging part. Since it is connected with neighboring ones only by rails and ballast in the actual structure, the constraint of the hanging part is weaker than that of other parts of RFVs. In particular, the Max value of DL-2 is larger than that of DL-4 although these points are both at the top of pier. That is because DL-2 is near the hanging part but DL-4 is far from the hanging part. The maximum acceleration response engenders a larger inertia force appears at the hanging part and then causes the increase of vibration response at DL-2. It is verified that the hanging part is the most important part of RFVs in which the HST can induce the serious vibration influence. Besides, the acceleration response of each point is close in the lateral direction. The probable reason is that the lateral excitation of TBI system mainly includes the lateral irregularity and then different sizes of lateral irregularity corresponding to the observation point induce the difference of acceleration responses in the lateral direction.

About vibration frequency, all of observation points basically have the similar frequency components in both vertical and lateral directions. Because the wavelength of one car length has the highest number of appearances, the frequency components are mainly determined by the wavelength of the repeated one car length 25 m and the train speed 270 km/h. Then, the primary frequency component is 3.0 Hz and the higher frequency components are integral multiples of 3.0 Hz, which agrees well with the predominant frequency in the field measurements by Miyashita *et al.* (2007). It is indicated that the analytical results can well represent the frequency characteristics of HST-induced vibrations. Furthermore, it is shown that the amplitudes of Fourier spectra are different and show the variation of vibration intensity versus frequency components at different points. In the vertical direction, the Fourier spectra show distinct peaks of bridge vibration around 10 and 20 Hz, the amplitudes are obviously different for different points and the vibration responses are mainly caused by the lower frequency band especially at the hanging parts.

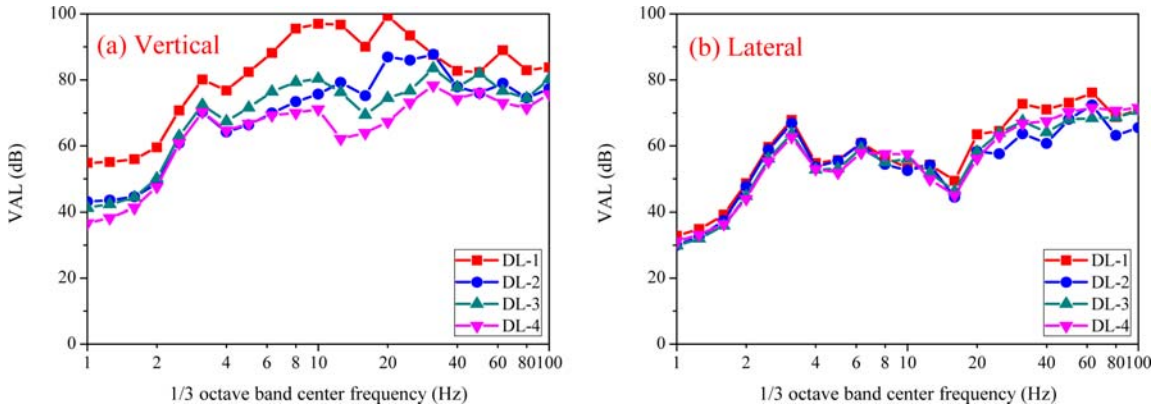

Figure 7. 1/3 octave band spectra of acceleration responses in the down line.

Table 4. Overall VALs of the RFVs (Unit: dB)

Direction	Down Line				Up Line			
	DL-1	DL-2	DL-3	DL-4	UL-1	UL-2	UL-3	UL-4
Vertical	101.61	89.71	87.40	82.13	98.30	82.88	76.49	75.15
Lateral	78.62	74.95	75.70	77.05	78.71	74.53	77.13	76.66

But in the lateral direction, the Fourier spectra are similar and the vibration responses are mainly caused by the higher frequency band for different points. The probable reason is that the gravity loads of HST mainly produce the lower frequency vibration but the track irregularities easily cause the higher frequency vibration in both vertical and lateral directions.

4.2. One-third octave band spectra

The vibration responses of RFVs are evaluated by the VALs obtained from 1/3 octave band spectral analysis as shown in Fig. 7. It is shown that all of 1/3 octave band spectra have the same primary frequency component 3.15 Hz with respect to the first peak value. It also denotes the primary frequency component 3.0 Hz in Fourier spectra. The variation curves have the similar variation tendency in the lower frequency band but some differences in the higher frequency band for the different points. Their vertical VALs at the hanging parts are larger than those at other parts and their predominant frequency components are basically in the low frequency band such as around 10 and 20 Hz. The lateral VALs are some difference for different points because different lateral irregularities are at different points. Their predominant frequency components are in the high frequency band such as around 31.5 and 60 Hz. Therefore, it is clarified that the primary frequency component of bridge vibration is dominated by the effect of periodic train loads with respect to the speed of the HST but their higher frequency components are mainly caused by track irregularities in both vertical and lateral directions.

The overall VALs of different observation points are shown in Table 4. It is indicated that the overall VALs in the vertical direction are much larger than those in the lateral direction especially in the down line. The overall VALs in the down line are larger than those of corresponding points in the up line in the vertical direction, but they are very close for different points in the lateral direction. The reason is that the excitations are different in the vertical and lateral directions. The excitations include the running HST modeled as multi-DOFs vibration system and the rails with simulated track irregularities. In particular, the HST is assumed to run along the down line and the same lateral irregularities are adopted in both left and right rails in the down line. Therefore, it is reconfirmed that the vibration influence in the vertical direction is stronger than that in the lateral direction and the vibration intensity at the hanging part is larger than other parts of RFVs.

5. Influential Parameter Analysis of Bridge Vibration

In this study, in order to clarify the vibration influence of various impact factors for the RFVs subjected to running HSTs and then explore the method of vibration mitigation, the influential parameter analyses are carried out with considering the TBI. In general, the vibration responses of TBI system in both vertical and lateral directions are influenced by a number of factors mainly including three aspects: the HST, track structure and the RFV. Therefore, the impact factors including train speed, train type, track irregularity, rail type and damping are investigated by means of the developed 3D numerical analysis approach. Since the hanging part is the most important part of RFVs for the bridge vibration, the vibration responses of the hanging part are taken as the main discussion objectives

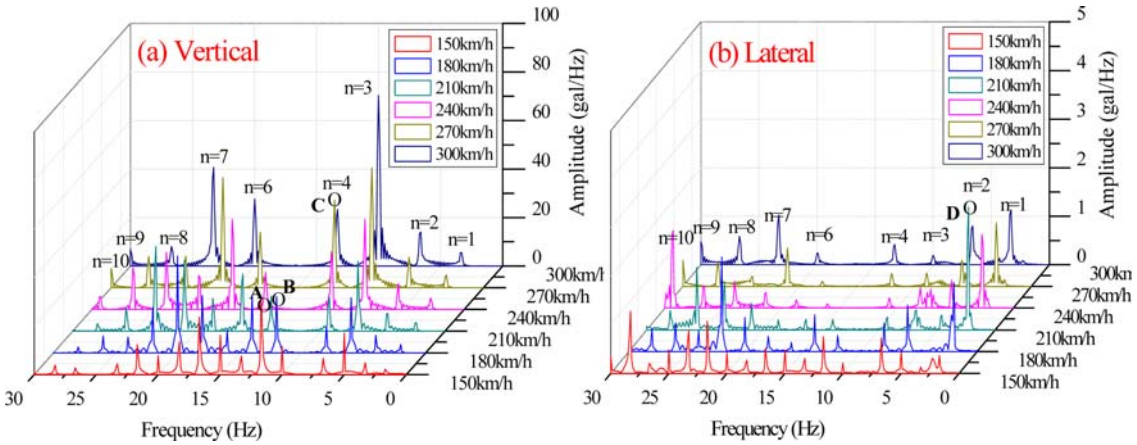

Figure 8. Variation of bridge vibration with train speeds in the frequency domain (DL-1).

to evaluate the parametric effects of bridge vibration.

5.1. Effect of train speed

The train speed is the most important impact factor influencing the vibration responses in the railway bridges. With the improving of speed of the HST, understanding the vibration behavior of TBI system becomes more and more important. It is necessary to investigate the vibration influence of RFVs at different speeds for the purpose of safe running and comfortable riding. The bridge vibration varies with train speed in the frequency domain as shown in Fig. 8. These results show clear spectrum peaks corresponding to vibration frequencies in this frequency domain. The vibration frequencies are mainly determined by the wavelength of the repeated wheel loading, i.e. the distance between two wheelsets. From the wavelengths of all the possible combinations of wheelsets and the number of repeated passing times for each HST, it is found that the wavelength of one car length (L=25 m) has the highest number of appearances. Hence, if the HST passes the RFVs with a speed of v (m/s), the dominant frequencies of bridge vibration induced by running HSTs are calculated using as follows.

$$f_n = n f_1 = nv/L = nV/90 \tag{20}$$

Higher frequency components f_n are integral multiples of the primary frequency component f_1 of bridge vibration. The dominant frequency for a certain n is linearly proportional to the train speed v because the car length L is constant for the specific HST. The fast HST has a shorter duration time but induces a larger vibration magnitude in a linear relationship with the train speed except when there is resonance. A longer duration time may increase vibration near the resonance condition, but damping will restrict the vibration magnitude. The high-frequency vibration is damped faster than the low-frequency vibration. The bridge vibration along the dominant frequency lines is apparently large in the vertical and lateral directions as shown in Fig. 8. But the bridge vibration is zero when n is equal to 5, that is because of the arrangement of the wheelsets of HST. Thus, the bridge vibration is dominated by the frequency of train loads not only in the vertical direction but also in the lateral direction although train loads are mainly in the vertical direction. Peaks A, B and C resonate with the train loads at the frequency components $7V/90$ (V=150 km/h), $6V/90$ (V=180 km/h) and $4V/90$ (V=270 km/h) near the vertical natural frequency (11.9 Hz) of RFVs. Peak D resonates with the train loads at the frequency component $V/90$ (V=210 km/h) near the lateral natural frequency (2.2 Hz) of RFVs. It is indicated that the train loads at the dominant frequency of RFVs with a smaller n often produce larger bridge vibration under the resonance condition. When the resonance frequency is constant, a larger n will cause a smaller train speed V and decrease the resonance vibration of RFVs. Therefore, to avoid the resonance of TBI system, the dominant frequencies of train loads should be different from the natural frequencies of the RFVs.

The maximum accelerations of different observation points generally increase with the increase of train speed for the overall trend in both vertical and lateral directions as shown in Fig. 9. The maximum accelerations in the vertical direction are much larger than those in the lateral direction. For the different observation points, the vibration behaviors are similar in trend but different in magnitude due to different positions. In particular, the vertical maximum acceleration at the hanging part DL-1 is much larger than those of other parts. It is found that the vibration responses of hanging parts are predominated for the whole bridge vibration in the vertical direction. But in the lateral direction, the whole bridge vibration is not related to the vibration responses of hanging parts and they mainly depend on the respective lateral irregularities of observation points. Therefore, it is useful to mitigate the vertical vibration responses of RFVs through controlling the vibration responses at the hanging parts, but it is difficult to mitigate the lateral bridge vibration.

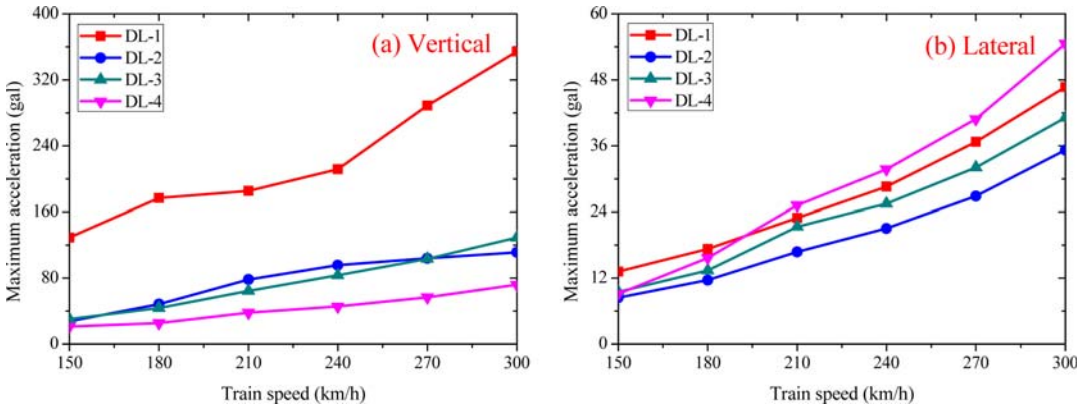

Figure 9. Effect of train speeds on maximum accelerations in the down line.

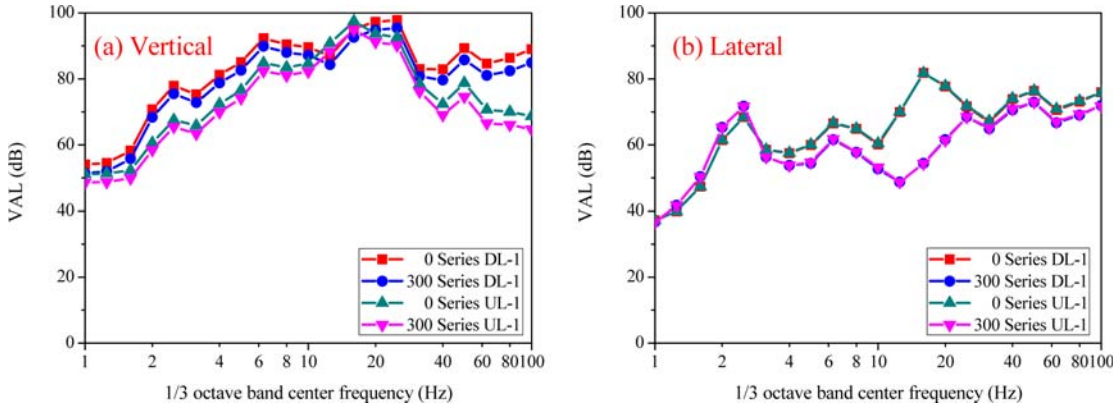

Figure 10. 1/3 octave band spectra of bridge vibration for different train types (210 km/h).

5.2. Effect of train type

With the rapid development of Shinkansen trains, the train type is upgraded quickly for the lighter and the faster train. In this study, 0 and 300 Series are taken as the comparative objects to discuss the vibration responses of RFVs induced by running HSTs. The axle load of 0 and 300 Series is 15.09 and 11.33 t, respectively. The vibration properties of 0 and 300 Series are shown in Table 1. The 1/3 octave band spectra for different train types at the speed of 210 km/h in both vertical and lateral directions are shown in Fig. 10. It is shown that the VALs at the hanging part are similar in trend but different in magnitude between 0 and 300 Series. The vertical VALs for 300 Series are somewhat smaller than those for 0 Series. That is mainly because the axle load of 300 Series is smaller than that of 0 Series. Except 12.5 and 16 Hz, the VALs at DL-1 are larger than those at UL-1 because the HST is assumed to run along the down line. The lateral VALs for 300 Series are also smaller than those for 0 Series but the VALs at DL-1 are the similar with those at UL-1. The probable reason is that the train loads are different between 0 and 300 Series but the lateral irregularities are same for both left and right rails. In particular, the VALs around 16 Hz for 0 Series are much larger than those for 300 Series. The probable reason is that 0 Series induces the resonance vibration of RFVs at 16 Hz. Through comparing the overall VALs for 0 Series, the overall VALs for 300 Series decrease about 2.51-3.76 and 4.18-6.35 dB in the vertical and lateral direction, respectively. Therefore, it is verified that the light weight train can effectively reduce the vibration responses of RFVs in both vertical and lateral directions.

The maximum accelerations of hanging parts for different train types in both vertical and lateral directions are shown in Fig. 11. It is shown that the maximum accelerations are basically similar in trend but different in magnitude between 0 and 300 Series. Especially, the maximum accelerations for 0 Series are magnified at the speed of 150 km/h. The maximum accelerations for 0 Series are larger than those for 300 Series in both vertical and lateral directions. The main reason is that the axle load of 0 Series is much larger than that of 300 Series. Then, the maximum acceleration at DL-1 is larger than that at UL-1 in the vertical direction but they are close in the lateral direction. That is because the HST is assumed to run along the down line and the lateral irregularity is same for the left and right rails. Therefore, it is very useful to mitigate the HST-induced vibrations of TBI system by the development of light weight of train.

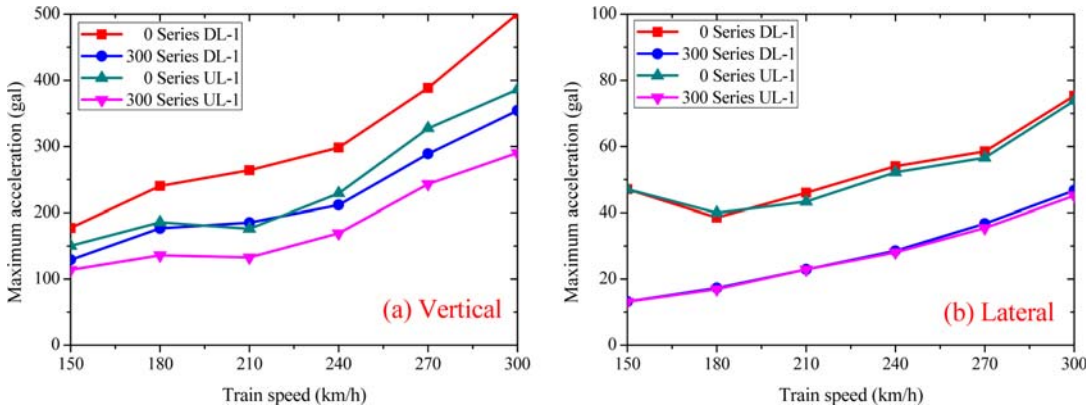

Figure 11. Effect of train types on maximum acceleration for bridge vibration.

5.3. Effect of track irregularity

The track irregularity is an important interference source of the HST-induced vibration and one of the main influential factors to control the highest speed of HST. The strong bridge vibration can not only influence the working state and serviceability of the bridge, but also reduce the traveling stability, comfort and safety of the train. Whether good track irregularity can be obtained or not is one of key problems to determine the high-speed railway success or fail. Regarding this topic, one aspect is that the established track irregularity spectrum is used to study the influence of TBI system with different time samples; the other aspect is that different kinds of track irregularity spectra are used to study the dynamic property of the train. In general, the actual measured track irregularity record is necessary if a simulation is expected to give a real response result and capture the influence of track irregularity. However, such a record is not always available for high-speed railway considered in a simulation. Another solution is to use the PSD function for the track geometry in the frequency domain to represent the track irregularity. Therefore, German track irregularity spectra are taken as comparative objects to clarify the vibration influence of track irregularity for the TBI system.

German track irregularity spectra are composed of high disturbance and low disturbance as shown in Fig. 12. Low disturbance is suitable for the high-speed railway allowable velocity above 250 km/h. High disturbance is suitable for the general railway. The PSD functions of track irregularities in both vertical and lateral directions are adopted as Eqs. (21) and (22), respectively.

$$S_v(\Omega) = \frac{A_v \cdot \Omega_c^2}{(\Omega^2 + \Omega_r^2)(\Omega^2 + \Omega_c^2)} \quad \text{m}^2/(\text{rad/m}) \tag{21}$$

$$S_a(\Omega) = \frac{A_a \cdot \Omega_c^2}{(\Omega^2 + \Omega_r^2)(\Omega^2 + \Omega_c^2)} \quad \text{m}^2/(\text{rad/m}) \tag{22}$$

where, Ω (rad/m) indicates the spatial circular frequency of the track irregularity; Ω_c and Ω_r (rad/m) are the cut off frequency; A_v and A_a ($\text{m}^2\cdot\text{rad/m}$) are the roughness constant. The values of the cut off frequency and the roughness constant are shown in Table 5. The wavelength properties are shown in Fig. 12, which can satisfy the vibration analysis of TBI system in the wavelength range from 1 to 100 m. It is shown that low disturbance is better than high disturbance. In general, the short wave components affect the running safety indices such as derailment factors and offload factors, while the long wave components affect the car-body accelerations and the riding comfort of passengers. Then, the stochastic process time samples simulated by the frequency domain method are adopted to discuss the vibration influence of track irregularities for the RFVs.

Table 5. Cut off frequency and roughness constant

Track grade	Low disturbance	High disturbance
Ω_c/(rad/m)	0.8246	0.8246
Ω_r/(rad/m)	0.0206	0.0206
A_a/($\text{m}^2\cdot$rad/m)	2.119×10^{-7}	6.125×10^{-7}
A_v/($\text{m}^2\cdot$rad/m)	4.032×10^{-7}	10.80×10^{-7}

The 1/3 octave band spectra for different track irregularities at the speed of 240 km/h are shown in Fig. 13. It is shown that the frequency characteristics of RFVs are some difference between low disturbance and high disturbance. In the vertical direction, the variation tendency of VALs is same in the range from 1.6 to 20 Hz but it is different in the range from 20 to 100 Hz between low disturbance and high disturbance. The VALs caused by high disturbance are larger than those caused by low disturbance. That is because the low frequency vibration is dominated by the train loads but their high frequency vibration mainly caused by the track irregularities. The VALs at DL-1 are larger than those at UL-1. In the lateral direction, the VALs caused by high disturbance are somewhat larger than those caused by low disturbance but the VALs at DL-1 are the same with those at UL-1. In particular, high disturbance causes an obvious peak value at the center

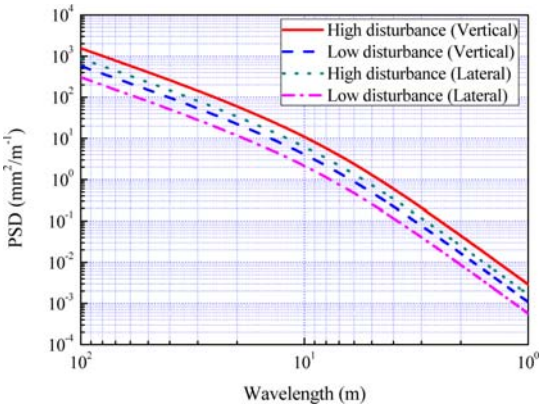

Figure 12. German track irregularity spectra.

frequency 8 Hz. The probable reason is that the resonance vibration of the RFVs is caused by high disturbance. Furthermore, it is indicated that the influence of lateral irregularity on the HST-induced vibration is more serious than that of vertical irregularity but the predominant frequency components are similar between low disturbance and high disturbance. The worse track irregularities can induce the larger vibration responses of RFVs in both vertical and lateral directions. Therefore, it is useful to the safe operation of the HST and the reduction of the HST-induced vibration through the improvement of track irregularities.

The maximum accelerations of hanging parts for different track irregularities in both vertical and lateral directions are shown in Fig. 14. It is indicated that the variation tendency is similar for low disturbance and high disturbance because of the same property of spatial frequency. The maximum accelerations caused by high disturbance are larger than those caused by low disturbance. The difference values of maximum accelerations between DL-1 and UL-1 become larger with increasing the train speeds for high disturbance in both vertical and lateral directions. But the difference values for low disturbance are smaller than those for high disturbance. The probable reason is that the worse track irregularity can induce the more serious train-bridge interaction and then the vibration responses of RFVs become larger with the increase of train speeds.

5.4. Effect of rail type

The rail type is as one of impact factors for the influence of vibration responses of TBI system. In recent years, the idea of such stiffer and heavier rails has already been applied to the railway system. In this study, 60 and 70 kg rail are mainly taken as the comparative objects to discuss the vibration responses of RFVs induced by

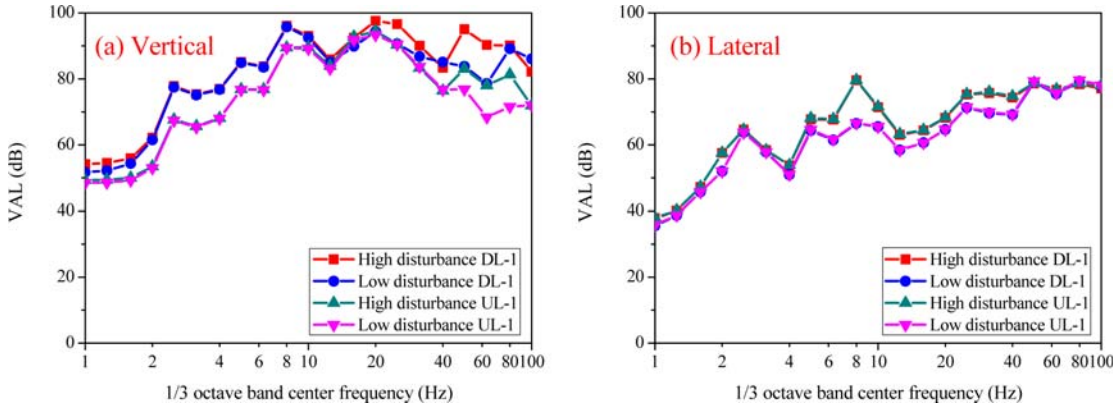

Figure 13. 1/3 octave band spectra of bridge vibration for different track irregularities (240 km/h).

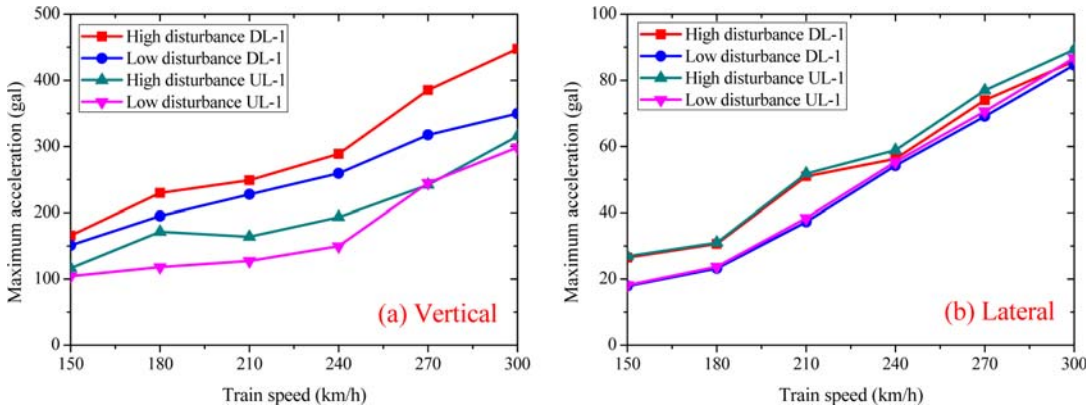

Figure 14. Effect of track irregularities on maximum acceleration for bridge vibration.

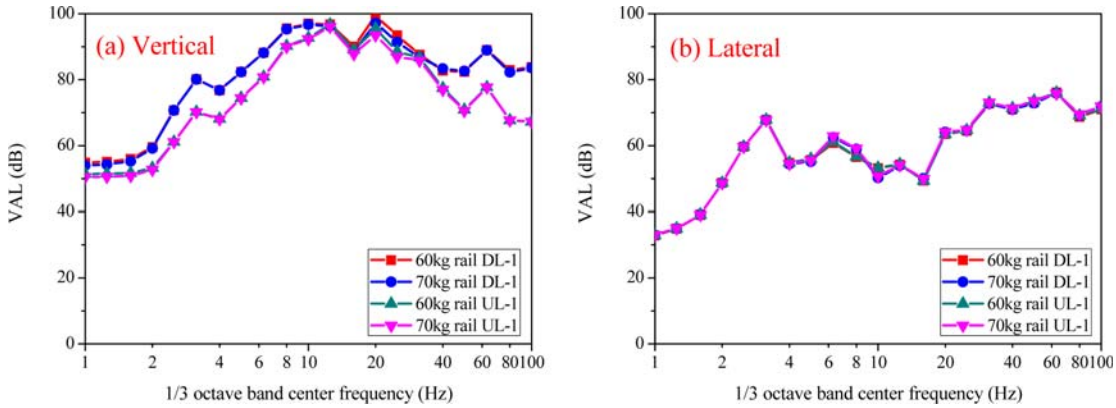

Figure 15. 1/3 octave band spectra of bridge vibration for different rail types (270 km/h).

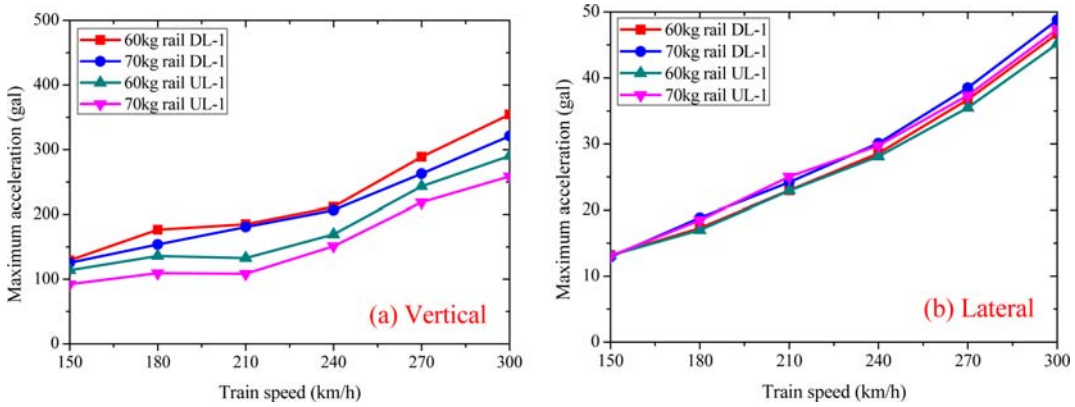

Figure 16. Effect of rail types on maximum acceleration for bridge vibration.

running HSTs. The structural properties of 60 and 70 kg rail are shown in Table 3. The 1/3 octave band spectra for different rail types at the speed of 270 km/h are shown in Fig. 15. It is shown that the VALs at the hanging parts are very close not only in trend but also in magnitude between 60 and 70 kg rail. Through comparing the overall VALs for 60 kg rail, the overall VALs for 70 kg rail decrease a little in the vertical direction but increase a little in the lateral direction. Therefore, it is difficult to reduce the HST-induced vibration of RFVs by using the stiffer and heavier rails. The maximum accelerations of hanging parts for different rail types in both vertical and lateral directions are shown in Fig. 16. It is shown that the maximum accelerations are also similar in trend but different in magnitude between 60 and 70 kg rail in both vertical and lateral directions. The vertical maximum accelerations for 70 kg rail are basically smaller than those for 60 kg rail. In particular, the vertical maximum accelerations at DL-1 are close between 60 and 70 kg rail for some train speeds. The lateral maximum accelerations for 70 kg rail are somewhat larger than those for 60 kg rail. It is indicated that the vibration influence for different rail types is very small in both vertical and lateral directions.

5.5. Effect of damping

Damping is the important impact factor to influence the vibration responses of TBI system. It is a desirable property of structural materials and forms which can reduce the HST-induced vibration and cause the bridge structures to reach their state of equilibrium soon after the HST or other excitation. For the bridge structures, the sources of damping are both internal and external. The internal sources of damping include the viscous internal friction of structural materials experienced during their deformation, their non-homogeneous properties, crack and so on. The external sources of damping include the friction in the supports, bearings, the permanent way, the ballast and the joints, the viscoelastic properties of soils and rocks below or beyond the bridge piers and so on. It is obvious that the number of sources of damping of bridge vibration is high in the high-speed railway and that it is almost impossible to take them all into account in engineering calculations. Therefore, the different damping ratios of RFVs such 1, 3, 5, and 7% are taken as the comparative objects to clarify the vibration influence of damping. The 1/3 octave band spectra for different damping ratios at the speed of 270 km/h are shown in Fig. 17. It is shown that the

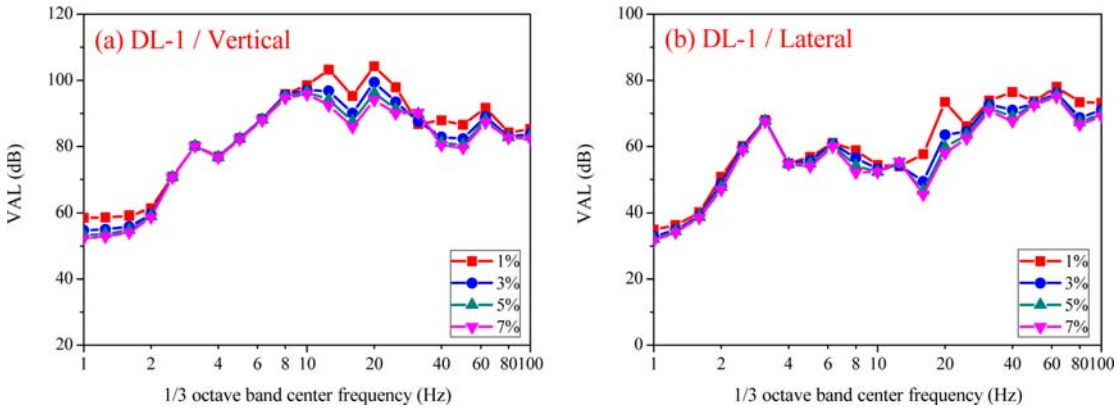

Figure 17. 1/3 octave band spectra of bridge vibration for different damping ratios (270 km/h).

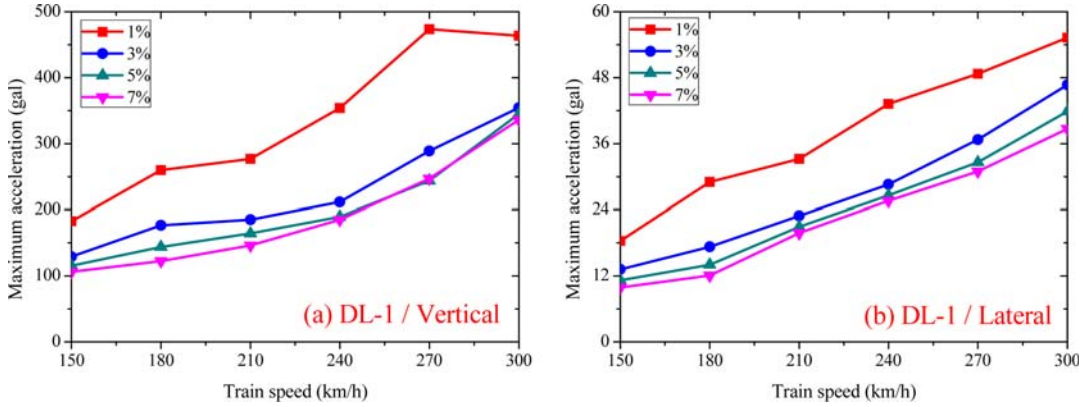

Figure 18. Effect of damping ratios of the viaducts on maximum acceleration for bridge vibration.

frequency characteristics of HST-induced vibration are similar in trend but different in magnitude for different damping ratios. All of 1/3 octave band spectra of each point have the same first peak value at the same center frequency 3.15 Hz and the same predominant frequency components for different damping ratios. Around the primary frequency component, the VALs are very close for different damping ratios. That is because the primary frequency component is determined by the speed of HST and the first peak value is mainly caused by the gravity loads of HST. It is indicated that the damping depends very little on vibration frequency in the region of low frequencies especially the primary frequency component and this is the range within which the RFVs vibrate most frequently. But around another predominant frequency component, the VALs are different and they decrease with the increase of damping ratio from 1 to 7%. It is shown that the HST-induced vibration of RFVs can be easily attenuated through increasing the damping of RFVs in the region of high frequency. The larger damping ratio can lead to reduce much more vibration responses. Therefore, it is useful to reduce the HST-induced vibration through increasing the damping of RFVs.

The maximum accelerations of hanging parts for different damping ratios are shown in Fig. 18. It is shown that the maximum accelerations are basically similar in trend but different in magnitude for different damping ratios. The vibration responses of RFVs increase with the increase of train speed but decrease with the increase of damping ratio of RFVs in both vertical and lateral directions. In particular, the variation tendency of vibration responses at the hanging parts for the damping ratio 1% is a little different in the vertical direction. It is indicated that the larger damping ratio can lead to much more reduction of maximum acceleration of RFVs in both vertical and lateral directions.

6. Concluding Remarks

In this study, the vibration characteristics and the parametric influences for the vibration responses of RFVs in both vertical and lateral directions caused by running HSTs are investigated by means of developed 3D numerical analysis approach. The impact factors including train speed, train type, track irregularity, rail type and damping are considered to clarify their effects for the TBI system. Based on the analytical results, the following conclusions are summarized.

(1) The vibration characteristics of RFVs are clarified in both vertical and lateral directions due to the running

HSTs. The vibration influence of RFVs in the vertical direction is more serious than that in the lateral direction. It is verified that the hanging part is the most important part of RFVs in which the HST can induce the serious vibration influence. The vibration responses at the hanging parts can cause the increase of vibration responses at other adjacent parts of RFVs. It is found that the predominant frequency components are similar for different observation points or directions and their corresponding amplitudes are different. The gravity loads of HSTs mainly induce the lower frequency vibration. The vertical and lateral irregularities mainly cause the higher frequency vibration in the vertical and lateral direction, respectively. In particular, the vertical overall VALs of the hanging parts are larger than those of other parts. Therefore, it is necessary to take action to control the vibration responses at the hanging parts to mitigate the excessive vibration of the RFVs.

(2) For train speed, it is the most important impact factor to influence the vibration responses of TBI system. The vibration frequency of RFVs is mainly dependent on the train speed in relation to the car length. The higher frequency components are integer multiples of the primary frequency component. The fast HST has a shorter duration time but induces a larger vibration magnitude in a linear relationship with the train speed except when there is resonance. A longer duration time may increase the vibration near the resonance condition, but damping will restrict the vibration magnitude. The high-frequency vibration is attenuated faster than the low-frequency vibration. The bridge vibration at the dominant frequencies (nv/L) is significantly large, not only in the vertical direction but also in the lateral direction, even though train loads are mainly in the vertical direction. Therefore, to avoid the resonance of TBI system, the dominant frequencies of the train loads should be different from the natural frequencies of the RFVs.

(3) For train type, the vibration responses of RFVs are influenced obviously by different train types. It is verified that the light weight train such as the decrease of axle loads and the improvement of vibration properties of the HST can effectively reduce the vibration responses of RFVs in both vertical and lateral directions.

(4) For track irregularity, the vibration responses of RFVs are also influenced by different track irregularities especially for the high-frequency vibration. The influence of lateral irregularity on the bridge vibration is more serious than that of vertical irregularity but the predominant frequency components are similar. It is indicated that the worse track irregularities can induce the larger vibration responses of RFVs in both vertical and lateral directions. It is useful to safe operation and vibration reduction by the improvement of track irregularities.

(5) For rail type, the vibration responses of RFVs are somewhat influenced by different rail types. It is difficult to reduce the vibration responses of RFVs in both vertical and lateral directions by using the stiffer and heavier rails.

(6) For damping, the vibration responses of RFVs are influenced by different damping ratios of RFVs. The HST-induced bridge vibration can be easily attenuated through increasing damping ratios of RFVs in the region of high frequency. It is indicated that the larger damping can lead to much more reduction of bridge vibration.

The results obtained in this study can not only clarify the vibration characteristics and parametric influences for the TBI system in both vertical and lateral directions due to the running HSTs, but also provide convenient predictions and diagnoses to the HST-induced vibrations of either existing bridges or those in the planning stage. It is also useful to understand the vibration influence for different conditions to develop effective countermeasures for mitigation the HST-induced vibrations.

Acknowledgment

This work was supported by fund from the National Natural Science Foundation of China (No: 51178365) and financially supported by self-determined and innovative research funds of WUT (No: 2010-YB-14).

References

Chen, G. and Zhai, W. M. (1999). "Numerical simulation of the stochastic process of railway track irregularities." *Journal of Southwest Jiaotong University*, 34(2), pp. 138-142.

Dinh, V. N., Kim, K. D., and Warnitchai, P. (2009). "Dynamic analysis of three-dimensional bridge-high-speed train interactions using a wheel-rail contact model." *Engineering Structures*, 31(12), pp. 3090-3106.

Frýba, L. (1996). *Dynamics of Railway Bridges*. Thomas Telford Ltd., London, UK.

Garinei, A. and Risitano, G. (2008). "Vibrations of railway bridges for high speed trains under moving loads varying in time." *Engineering Structures*, 30(3), pp. 724-732.

Guo, W. W., Xia, H., De Roeck, G., and Liu, K. (2012). "Integral model for train-track-bridge interaction on the Sesia viaduct: dynamic simulation and critical assessment." *Computers and Structures*, 112-113, pp. 205-216.

Ju, S. H., Lin, H. T., and Chen, T. K. (2007). "Studying characteristics of train-induced ground vibrations adjacent to an elevated railway by field experiments." *Journal of Geotechnical and Geoenvironmental Engineering*, ASCE, 133(10), pp. 1302-1307.

Kawatani, M., He, X. W., Shiraga, R., Seki, M., Nishiyama, S., and Yoshida, K. (2006). "Dynamic response analysis of elevated railway bridges due to Shinkansen trains." *Journal of Structural and Earthquake Engineering*, JSCE, 62(3), pp. 509-519.

Liu, K., Zhou, H., Shi, G., Wang, Y.Q., Shi, Y. J., and De Roeck, G. (2013). "Fatigue assessment of a composite railway bridge for high speed trains. Part II: Conditions for which a dynamic analysis is needed." *Journal of Constructional Steel Research*, 82, pp. 246-254.

Martínez-Rodrigo, M. D., Lavado, J., and Museros, P.

(2010). "Transverse vibrations in existing railway bridges under resonant conditions: single-track versus double-track configurations." *Engineering Structures*, 32(7), pp. 1861-1875.

Matsuura, A. (1976). "A study of dynamic behavior of bridge girder for high speed railway." *Journal of Structural and Earthquake Engineering*, JSCE, 32(12), pp. 35-47.

Matsuura, A. (1998). "Simulation for analysing direct derailment limit of running vehicle on oscillating tracks." *Journal of Structural and Earthquake Engineering*, JSCE, 15(1), pp. 63-72.

Miyashita, T., Ishii, H., Fujino, Y., Shoji, T., and Seki, M. (2007). "Understanding of high-speed train-induced local vibration of a railway steel bridge using laser measurement and its effect by train speed." *Journal of Structural Mechanics and Earthquake Engineering*, JSCE, 63(2), pp. 277-296.

Nishimura, A. (1990). "A study on integrity assessment of railway rigid frame bridge." *RTRI Report*, 4(9), pp. 33-36.

Olmos, J. M. and Astiz, M. A. (2013). "Analysis of the lateral dynamic response of high pier viaducts under high-speed train travel." *Engineering Structures*, 56, pp. 1384-1401.

Rezvani, M. A., Vesali, F., and Eghbali, A. (2013). "Dynamic response of railway bridges traversed simultaneously by opposing moving trains." *Structural Engineering and Mechanics*, 46(5), pp. 713-734.

Su, D., Fujino, Y., Nagayama, T., Hernandez Jr, J. Y., and Seki, M. (2010). "Vibration of reinforced concrete viaducts under high-speed train passage: measurement and prediction including train-viaduct interaction." *Structure and Infrastructure Engineering*, 6(5), pp. 621-633.

Sun, L. M. (2014). *Study on environmental vibration and mitigation countermeasures caused by running high-speed train on railway viaduct*. Doctoral Dissertation, Hokkaido University, Sapporo, Japan.

Takemiya, H. and Bian, X. C. (2007). "Shinkansen high-speed train induced ground vibrations in view of viaduct-ground interaction." *Soil Dynamics and Earthquake Engineering*, 27(6), pp. 506-520.

Tanabe, M., Wakui, H., Matsumoto, N., Okuda, H., Sogabe, M., and Komiya, S. (2003). "Computational model of a Shinkansen train running on the railway structure and the industrial applications." *Journal of Materials Processing Technology*, 140(1-3), pp. 705-710.

Uno, M., Sogabe, M., Tanimura, Y., and Kanamori, M. (2007). "A study on dynamic response of the railway continuous girder by running high-speed train." *Journal of Structural Engineering*, JSCE, 53A, pp. 67-76.

Wakui, H., Matsumoto, N., Matsuura, A., and Tanabe, M. (1995). "Dynamic interaction analysis for railway vehicles and structures." *Journal of Structural and Earthquake Engineering*, JSCE, 51(8), pp. 129-138.

Xia, H., De Roeck, G., and Goicolea, J. M. (2012). *Bridge Vibration and Controls: New Research*. Nova Science Publishers, New York, USA.

Xia, H., Gao, F., Wu, X., Zhang, N., De Roeck, G., and Degrande, G. (2009). "Running train induced vibrations and noises of elevated railway structures and their influences on environment." *Frontiers of Architecture and Civil Engineering in China*, 3(1), pp. 9-17.

Xie, W. P. and Xu, W. (2012). "Vehicle-induced vibration responses of a rail box girder in Wuhan station." *Journal of Vibration and Shock*, 31(8), pp. 186-190.

Yang, Y. B. and Lin, C. W. (2005). "Vehicle-bridge interaction dynamics and potential applications." *Journal of Sound and Vibration*, 284(1-2), pp. 205-226.

Yang, Y. B., Yau, J. D., and Wu, Y. S. (2004). *Vehicle-bridge interaction dynamics: with applications to high-speed railways*. World Scientific, Singapore.

Yokoshima, S. and Tamura, A. (1999). "A study on factors constituting annoyance due to Shinkansen railway vibration." *Journal of Architecture, Planning and Environmental Engineering*, AIJ, No. 526, pp. 1-7.

Zhou, H., Liu, K., Shi, G., Wang, Y.Q., Shi, Y.J., and De Roeck, G. (2013). "Fatigue assessment of a composite railway bridge for high speed trains. Part I: Modeling and fatigue critical details." *Journal of Constructional Steel Research*, 82, pp. 234-245.